

NONLINEAR OPTICAL PHENOMENA

PACS numbers: 42.62.Eh; 42.65.Dr; 42.65.Lm; 42.70.Mp
DOI: 10.1070/QE2014v044n11ABEH015356

Theoretical study of collinear optical frequency comb generation under multi-wave, transient stimulated Raman scattering in crystals

S.N. Smetanin

Abstract. **Using mathematical modelling we have studied the conditions of low-threshold collinear optical frequency comb generation under transient (picosecond) stimulated Raman scattering (SRS) and parametric four-wave coupling of SRS components in crystals. It is shown that Raman-parametric generation of an octave-spanning optical frequency comb occurs most effectively under intermediate, transient SRS at a pump pulse duration exceeding the dephasing time by five-to-twenty times. We have found the optimal values of not only the laser pump pulse duration, but also of the Raman crystal lengths corresponding to highly efficient generation of an optical frequency comb from the second anti-Stokes to the fourth Stokes Raman components. For the $KGd(WO_4)_2$ (high dispersion) and $Ba(NO_3)_2$ (low dispersion) crystals pumped at a wavelength of 1.064 μm and a pulse duration five or more times greater than the dephasing time, the optimum length of the crystal was 0.3 and 0.6 cm, respectively, which is consistent with the condition of the most effective Stokes–anti-Stokes coupling $\Delta kL \approx 15$, where Δk is the wave detuning from phase matching of Stokes–anti-Stokes coupling, determined by the refractive index dispersion of the SRS medium.**

Keywords: *stimulated Raman scattering, optical frequency comb, four-wave mixing, wave detuning, dephasing time.*

1. Introduction

Stimulated Raman scattering (SRS) is an effective method for the frequency shift of laser radiation. It is well known [1] that the SRS process can be cascaded, resulting in the generation of many Stokes SRS components shifted relative to each other by the Raman frequency, which is a parameter of an SRS medium. The SRS process in crystals is due to complex vibrations of the crystal lattice, which provides a set of Raman frequencies with a shift of about 1000 cm^{-1} for the most intense Raman lines [2]. Cascaded SRS in crystals at various Raman frequencies can ensure optical frequency comb generation for the synthesis of ultrashort light pulses in metrology. However, implementation of cascade generation of high-order Stokes SRS components in crystals is hindered due to a sharp drop of the SRS gain with increasing wavelength of light [3], and with respect to the intensity it is limited by the damage threshold of the SRS crystal.

The presence of parametric four-wave coupling of SRS components can significantly reduce and bring closer their generation thresholds due to the fact that they originate from intense parametric rather than spontaneous seed radiation [4]. With such a Raman-parametric conversion, both Stokes and anti-Stokes SRS components can be generated. Four-wave (four-photon) generation of SRS components, unlike cascaded two-photon SRS generation, requires phase matching, which is prevented by the refractive index dispersion of the medium. Therefore, the multi-wave SRS generation often makes use of low-dispersion gases [5–8]. In crystals the generation of an octave-spanning frequency comb at Raman-parametric conversion of light was realised in [9–13].

In most cases, Raman-parametric generation is noncollinear. For example, the so-called anti-Stokes cones are generated [14], which is due to the maintenance of phase matching of four-wave mixing (FWM) of SRS components of radiation. Chiao and Stoicheff [15] were the first to describe quantitatively the mechanism of noncollinear Raman-parametric generation by the phase-matching conditions $\boldsymbol{k}_L + \boldsymbol{k}_{n-1} = \boldsymbol{k}_S + \boldsymbol{k}_n$, where $\boldsymbol{k}_L$ and $\boldsymbol{k}_S$ are the wave vectors of the laser pump and the first Stokes SRS components; and $\boldsymbol{k}_n$ and $\boldsymbol{k}_{n-1}$ are the wave vectors of the anti-Stokes SRS component of the nth and $(n-1)$th order, respectively ($n = 1, 2, 3,\ldots$; $\boldsymbol{k}_0 \equiv \boldsymbol{k}_L$), which made it possible to calculate the angles of the anti-Stokes cones in good agreement with experimental results for the calcite crystal. This phase matching condition takes into account not all possible FWM processes, but only those that involve the two most intense frequency components – pump wave ($\boldsymbol{k}_L$) and first Stokes component ($\boldsymbol{k}_S$). This approximation is valid in the case of self-matching during the noncollinear propagation of SRS components when four-wave interactions involving the most intense components have the greatest effect. Subsequently, this condition was used for the theoretical description of Raman-parametric generation in gases [16, 17]. However, noncollinear Raman-parametric generation has not yet found practical application in the synthesis of ultrashort light pulses, where collinear optical frequency comb generation is required.

Butylkin et al. [18, 19] showed that SRS in gases can be also characterised by collinear (axial) Raman-parametric generation, which is explained by the spatially limited phase capture of parametrically coupled waves during the FWM detuning of phase matching. Basiev et al. [4] analysed the influence of parametric coupling of different frequency components on the SRS threshold in solids as a function of the wave detuning of FWM and material dispersion. It was assumed that the

S.N. Smetanin A.M. Prokhorov General Physics Institute, Russian Academy of Sciences, ul. Vavilova 38, 119991 Moscow, Russia; e-mail: ssmetanin@bk.ru

Received 27 November 2013; revision received 16 May 2014
Kvantovaya Elektronika **44** (11) 1012–1021 (2014)
Translated by I.A. Ulitkin

detuning of the collinear FWM phase matching is due to the refractive index dispersion, which has the greater impact, the more the difference of frequencies of the interacting waves, i.e., the smallest wave detuning is exhibited by the processes of four-wave coupling of neighbouring SRS components. In this connection, Basiev et al. [4] took into account FWM of any neighbouring SRS components rather than FWM with the participation of the pump wave and the first Stokes components (these most intense components in the case of the collinear FWM do not dominate due to phase mismatching). The study was conducted for the steady-state SRS, although most experimental papers [9–13, 20, 21] make use of picosecond pumping.

In this paper we have investigated theoretically the conditions of low-threshold collinear optical frequency comb generation under transient (picosecond) SRS and parametric four-wave coupling of SRS components in crystals.

2. Theory

Transient collinear interaction of radiation with an SRS medium can be described by the coupled equations [22]:

$$\frac{\partial^2 E}{\partial z^2} - \frac{1}{c^2}\frac{\partial^2(\varepsilon E)}{\partial t^2} = \frac{4\pi}{c^2} N \frac{\partial \alpha}{\partial Q}\frac{\partial^2 (QE)}{\partial t^2}, \tag{1}$$

$$\frac{\partial^2 Q}{\partial t^2} + \frac{1}{\tau}\frac{\partial Q}{\partial t} + \Omega^2 Q = \frac{1}{2m}\frac{\partial \alpha}{\partial Q} E^2, \tag{2}$$

where E is the electrical field strength of radiation; Q is the vibration amplitude of an SRS medium; $\Omega = 2\pi\nu_R c$ is the centre frequency of vibrations; ν_R is the Raman frequency, measured in cm^{-1}; τ is the dephasing time of medium vibrations; m and N are the effective mass and concentration of vibrating particles; $\partial\alpha/\partial Q$ is the coefficient of variation in the medium polarisability; and ε is the medium permittivity.

Many SRS components are involved in this interaction, i.e.

$$E = \frac{1}{2}\sum_j E_j \exp(\mathrm{i}\omega_j t - \mathrm{i}k_j z) + \text{c.c.}, \tag{3}$$

where E_j is the slowly varying complex amplitude of the jth SRS component ($j = 0$ is the pump wave, $j > 0$ are the Stokes SRS components, and $j < 0$ are the anti-Stokes SRS components); and ω_j and k_j are its frequency and wave number.

The constitutive equation (2) has the squared electric field strength that, taking expression (3) into account, can be written as

$$E^2 \approx \frac{1}{2}\sum_j E_j E^*_{j+1} \exp[\mathrm{i}(\omega_j - \omega_{j+1})t - \mathrm{i}(k_j - k_{j+1})z] + \text{c.c.}, \tag{4}$$

which takes into account only those terms that describe the resonant excitation of SRS vibrations of a medium. The vibration amplitude of the medium excited by light of squared field strength (4), can be written as:

$$Q \approx \frac{1}{2}\sum_j q_{j,j+1} \exp[\mathrm{i}(\omega_j - \omega_{j+1})t - \mathrm{i}(k_j - k_{j+1})z] + \text{c.c.}, \tag{5}$$

where $q_{j,j+1}$ is the slowly varying complex vibration amplitude of the medium excited by the waves E_j and E_{j+1}. Substitution of (4) and (5) into equation (2) in the case of exact resonance ($\omega_j - \omega_{j+1} = \Omega$) gives the constitutive equations for slowly varying amplitudes of light waves (E_j) and medium vibrations ($q_{j,j+1}$):

$$\frac{\partial q_{j,j+1}}{\partial t} + \frac{1}{2\tau} q_{j,j+1} = -\frac{\mathrm{i}}{4m\Omega}\frac{\partial \alpha}{\partial Q} E_j E^*_{j+1}. \tag{6}$$

Substituting expressions (3) and (5) into the wave equation (1) yields a system of coupled truncated wave equations for each jth SRS component:

$$\begin{aligned}
\frac{\partial E_j}{\partial z} + \frac{1}{u_j}\frac{\partial E_j}{\partial t} = -\mathrm{i}\frac{\pi\omega_j^2}{k_j c^2} N \frac{\partial \alpha}{\partial Q}[&E_{j-1} q^*_{j-1,j} + E_{j+1} q_{j,j+1} \\
&+ E_{j+1} q_{j+1,j+2} \exp(\mathrm{i}\Delta k_{j+1} z) + E_{j-1} q^*_{j-2,j-1} \exp(\mathrm{i}\Delta k_{j-1} z) \\
&+ (E_{j-1} q^*_{j,j+1} + E_{j+1} q_{j-1,j}) \exp(-\mathrm{i}\Delta k_j z) \\
&+ E_{j+1} q_{j+2,j+3} \exp(\mathrm{i}\Delta K_{j+1} z) + E_{j-1} q^*_{j-3,j-2} \\
&\times \exp(\mathrm{i}\Delta K_{j-2} z) + E_{j-1} q^*_{j+1,j+2} \exp(-\mathrm{i}\Delta K_j z) \\
&+ E_{j+1} q^*_{j-2,j-1} \exp(-\mathrm{i}\Delta K_{j-1} z)],
\end{aligned} \tag{7}$$

where u_j is the group velocity of the jth SRS component propagation; Δk_j and ΔK_j are the wave detunings of partially degenerate and nondegenerate jth-order FWM processes, respectively. Three neighbouring SRS components with the subscripts $j - 1$, j and $j + 1$ are involved in the process of partially degenerate (two of the four interacting waves have the same frequency) jth-order FWM, and four neighbouring SRS components with the subscripts $j - 1$, j, $j + 1$ and $j + 2$ are involved in the nondegenerate jth-order FWM process. In the square brackets of equations (7) we have taken into account all the terms that satisfy the law of conservation of energy in the generation of the jth SRS component.

It should be noted that we consider here only FWM of neighbouring SRS components and neglect the four-wave coupling of nonadjacent SRS components, for which the frequencies of the interacting waves are very different, and therefore the sensitivity to the wave mismatch of FWM is high due to the large dispersion of the refractive index of SRS crystals. This allows us to describe in a single model almost all possible processes of four-wave coupling of the neighbouring SRS components.

As shown in [4], the contribution of the parametric coupling in SRS depends on the condition of phase matching of partially degenerate FWM of type $2\boldsymbol{k}_j = \boldsymbol{k}_{j-1} + \boldsymbol{k}_{j+1}$, where j is the number of the SRS radiation component, which is the FWM-pump wave ($j < 0$ is the anti-Stokes wave, $j > 0$ is the Stokes wave and $j = 0$ is the SRS-pump wave); $\boldsymbol{k}_j$ is the FWM-pump wave vector; and $\boldsymbol{k}_{j-1}$ and $\boldsymbol{k}_{j+1}$ are the vectors of neighbouring SRS components, which are the signal and idler waves of the jth process of partially degenerate FWM. Note that the SRS-pump ($j = 0$) and FWM-pump waves do not generally coincide. The presence of a wave detuning

$$\Delta k_j = k_{j-1} + k_{j+1} - 2k_j, \tag{8}$$

where k_j, k_{j-1} and k_{j+1} are moduli of the corresponding wave vectors, leads to violation of the wave matching condition, which weakens their parametric coupling.

The main reason for the wave detuning (8) is the dispersion of the refractive index of the medium. In this case, the wave detuning is defined as [meaning that $k_j = 2\pi n_j \lambda_j^{-1}$, $\lambda_j = (\lambda_0^{-1} - j\nu_R)^{-1}$]

$$\Delta k_j = (n_{j-1} + n_{j+1} - 2n_j)2\pi\lambda_j^{-1} + (n_{j-1} - n_{j+1})2\pi\nu_R, \qquad (9)$$

where λ_j is the FWM-pump wavelength; n_j, n_{j-1} and n_{j+1} are the refractive indices of the FWM-pump wave, signal wave and idler wave, respectively.

Apart from partially degenerate FWM, SRS is also accompanied by nondegenerate FWM having the wave matching of type $\boldsymbol{k}_j + \boldsymbol{k}_{j+1} = \boldsymbol{k}_{j-1} + \boldsymbol{k}_{j+2}$ [4], where $\boldsymbol{k}_j$ and $\boldsymbol{k}_{j+1}$ are the vectors of the first and second FWM-pump waves; and $\boldsymbol{k}_{j-1}$ and $\boldsymbol{k}_{j+2}$ are the vectors of the SRS components, which are the signal and idler waves of the nondegenerate FWM process. Wave detuning of nondegenerate jth-order FWM is defined as

$$\Delta K_j = (n_{j-1} + n_{j+2} - n_j - n_{j+1})2\pi\lambda_j^{-1}$$

$$+ (n_{j-1} + n_{j+1} - 2n_{j+2})2\pi\nu_R \approx \Delta k_j + \Delta k_{j+1}. \qquad (10)$$

Note that the system of equations (6) and (7) takes into account all possible processes of four-wave coupling of any neighbouring SRS components in the wave detuning of FWM phase matching, determined by the dispersion of the refractive index, in contrast to earlier models of multi-wave SRS [16, 17], where only some FWM processes necessarily involving the pump wave and the first Stokes component are considered.

The model is constructed in the approximation of collinearly generated plane waves and does not account for the conical waves, which, in practice, take over some of the pump energy. The model also does not take into account incomplete spatial overlap of SRS components. Therefore, this approximation does not make an attempt to determine the energy parameters of generated radiation. The SRS conversion efficiencies in the model turn out overestimated. However, we assume that the conditions of collinear SRS generation of optical frequency combs are described adequately, especially if we take into account the fact that conical waves are observed mainly in the anti-Stokes region of the spectrum and the spectrum of the generated frequency comb is more shifted to the Stokes region in which the waves are generated collinearly due to the cascade SRS process.

To initiate the process of cascade SRS generation, equation (6) should be modified, given that spontaneous Raman scattering yields the seed for SRS generation. There are two approaches.

In the first approach an additional term is introduced in equation (6) [23], which describes additional 'spontaneous' driving force of medium vibrations. This approach well describes the elementary process of SRS generation of a Stokes wave [24], but its use to describe the seed of cascade generation of many SRS components has not been substantiated in the literature. Raymer and Mostowski [24] also showed that the result of applying this approach in the steady-state case is close to that of the other (second) approach, which assumes that the medium initially has initiating spontaneous Stokes radiation. The second approach is used to describe not only the steady-state [25], but also transient SRS in the modelling of femtosecond SRS generation of a Stokes pulse from the noise in the pump field [26].

The second approach may be associated with the known experimental threshold condition of steady-state SRS $gI_L L \approx 25$ [27] (g is the SRS gain, I_L is the intensity of the laser pump at the input to the SRS medium and L is the length of the SRS medium) in which the SRS gain of the seed Stokes radiation $I_S(L) = I_{seed}\exp(gI_L L)$ occurs to the value of $I_S(L) \approx 0.01 I_L$ if the intensity of the seed Stokes radiation is $I_{seed} \approx 10^{-13} I_L$.

For us it is important that the second approach can justify cascade generation of many SRS components, where each Stokes SRS component is generated by pumping a previous SRS component, i.e. $I_{j+1}^{seed} \approx s^2 I_j$, where $s \approx \sqrt{10^{-13}}$ is the seed coefficient in the field amplitude, caused by spontaneous Raman scattering. Then, following [26], we replace in equation (6) the Stokes amplitude E_{j+1}^* by the sum of the generated and seed Stokes amplitudes $(E_{j+1}^* + S_{j+1}^*)$. Here we assume that $S_{j+1}^* = sE_j^*$, i.e., the noises of the $(j+1)$th components appear in the field of the jth component.

Calibration modelling in the second approach aimed at determining the seed for the pump pulse duration, which markedly exceeds the dephasing time, under the initial conditions corresponding to the conditional SRS threshold ($gI_L L \approx 25$) has shown, as expected, that the efficiency of SRS generation is equal to ~1% (if we do not take into account four-wave mixing of SRS components), and a two-fold increase in $gI_L L$ led to the overcoming of the lasing threshold of the second Stokes component (cascade process). When the seed coefficient s was increased by three times and $gI_L L$ was changed by no more than 10%, the output parameters of the calculation were the same. On the other hand, by setting (in accordance with the first approach) the same seed terms ($S_{j+1}^* = sE_0^*$) we have obtained in the calculations the generation pattern which is not very different from the previous case. The fact that SRS generation of the $(j+1)$th component is triggered at a large driving force of medium vibrations, which is proportional to $E_j E_{j+1}^*$ [see, equation (6)], i.e. when the amplitude of the jth component E_j is close to the pump amplitude E_0; therefore, the approaches considered yield similar results.

The presented model has recently been tested and showed agreement between the calculated results and the results of experiments on multi-wave picosecond SRS in crystals of simple tungstates at different lengths of SRS crystals [28].

3. Threshold of transient SRS

The problem of generation of high-order SRS components is associated with higher thresholds of their generation compared with the SRS formation threshold. Therefore, to find the conditions of low-threshold generation of many (anti-Stokes and Stokes) SRS components in the case of parametric coupling, it is first necessary to determine theoretically the threshold of transient SRS formation in the absence of generation.

Although in the absence of intrinsic losses the SRS process lacks the fundamental threshold effect, but in fact there is an experimental threshold caused by the fact that at the initial stage the SRS intensity rapidly increases exponentially.

For transient SRS in the case of undepleted pumping, according to [23, 29] the equations describing the two-photon SRS process [equations (6) and (7) at $j = 1$ and the absence of

FWM terms containing exponents] can be reduced to a self-consistent equation, which has the solution [29]:

$$|E(z,t')|^2 = |E(0,t')|^2 I_0^2\left(\sqrt{\frac{gz}{\tau}\int_{-\infty}^{t'} I_L(t)\,dt}\right)$$

$$\approx \frac{|E(0,t')|^2}{2\pi\sqrt{\frac{gz}{\tau}\int_{-\infty}^{t'} I_L(t)\,dt}}\exp\left(2\sqrt{\frac{gz}{\tau}\int_{-\infty}^{t'} I_L(t)\,dt}\right), \qquad (11)$$

where

$$g = \frac{8\pi^2\tau N_V\omega_1}{m\Omega c^2 n_0 n_1}\left(\frac{\partial\alpha}{\partial Q}\right)^2$$

is the SRS gain measured in cm W^{-1};

$$I_L(t') = \frac{cn_0}{8\pi}|E_0(t')|^2$$

is the laser pump pulse intensity measured in W cm^{-2}; and $n_{0,1}$ are the refractive indices for the pump wave and the Stokes wave, respectively.

It follows from (11) that under transient SRS the increase in the SRS radiation intensity is exponential, as in the case of steady-state SRS, but is slower. The increment of the exponential growth of the SRS radiation intensity at the output of the SRS medium ($z = L$) is determined (at $t_L \leqslant \tau$) as

$$G(t') = \ln\left(\frac{|E(L,t')|^2}{|E(0,t')|^2}\right)$$

$$\approx 2\sqrt{\frac{gL}{\tau}\int_{-\infty}^{t'} I_L(t)\,dt} - \ln\left(2\pi\sqrt{\frac{gL}{\tau}\int_{-\infty}^{t'} I_L(t)\,dt}\right). \qquad (12)$$

For a Gaussian laser pulse with a peak intensity I_L and a FWHM duration t_L, valid is the following expression

$$\int_{-\infty}^{\infty} I_L(t)\,dt = I_L t_L\sqrt{\frac{\pi}{4\ln 2}}.$$

Then, bearing in mind that $G(t') \to G_{max}$ at $t' \to \infty$, we obtain

$$G_{max} \approx 2\sqrt{gLI_L\frac{t_L}{\tau}\sqrt{\frac{\pi}{4\ln 2}}}$$

$$-\ln\left(2\pi\sqrt{gLI_L\frac{t_L}{\tau}\sqrt{\frac{\pi}{4\ln 2}}}\right). \qquad (13)$$

Threshold pump intensity I_L^{th} for observing SRS can be found by equating the maximum increment of the transient SRS gain G_{max} from expression (13) to the threshold value $G_{th} = 25$. For a Gaussian pulse of duration $t_L \leqslant \tau$ we obtain an implicit expression for the threshold pump intensity:

$$2\sqrt{gLI_L^{th}\frac{t_L}{\tau}\sqrt{\frac{\pi}{4\ln 2}}}$$

$$-\ln\left(2\pi\sqrt{gLI_L^{th}\frac{t_L}{\tau}\sqrt{\frac{\pi}{4\ln 2}}}\right) = 25. \qquad (14)$$

The second term in (14) is considerably smaller than the first one and thus I_L^{th} can be found by the approximation method. In the first approximation, we express I_L^{th} by neglecting the second term in (14), and in the second approximation we substitute the obtained value of I_L^{th} into the second term of the expression. We obtain the desired expression, which is valid at $t_L \leqslant \tau$:

$$gLI_L^{th} \approx \frac{[25 + \ln(25\pi)]^2}{4}\sqrt{\frac{4\ln 2}{\pi}}\frac{\tau}{t_L} \approx 203\frac{\tau}{t_L}. \qquad (15)$$

Note that the dependence of the threshold intensity I_L^{th} on τ/t_L is linear at $t_L \leqslant \tau$.

Figure 1 shows the dependences of the product gLI_L^{th} on the ratio τ/t_L – plotted by using the analytical formula (15) (dashed line) and numerical integration of equations (6) and (7) (points). For the points obtained by numerical integration, shown also is the linear approximation (solid curve) obtained by the least squares method (in the range of $\tau < t_L < 10\tau$ values) and defined by the expression

$$gLI_L^{th} \approx 22 + 207\tau/t_L. \qquad (16)$$

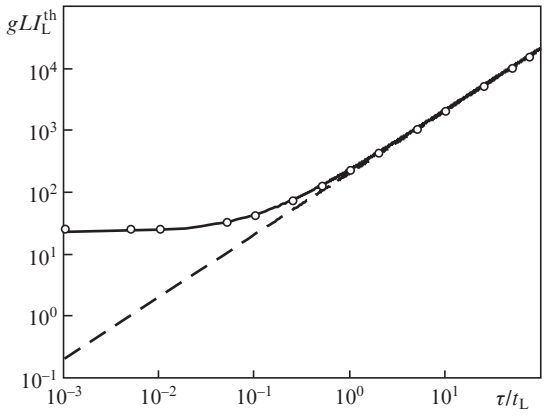

Figure 1. Dependences of gLI_L^{th} on τ/t_L, obtained by numerical integration of equations (6) and (7) (points) and plotted by the analytical formula (18) (dashed line), and the linear approximation of points obtained in the numerical integration in the range of $\tau < t_L < 10\tau$ values (solid curve).

One can see from Fig. 1 that formula (15) (dashed line) is in good agreement with the results of numerical calculation (points) in the $t_L \leqslant \tau$ ($\tau/t_L \geqslant 1$) region. It should be noted that the dependence obtained by numerical calculation (points) is close to linear in the $t_L > \tau$ region as well. The result of the linear approximation is consistent with the results of numerical calculation not only in the approximation region ($\tau < t_L < 10\tau$), but virtually in the entire range of τ/t_L values.

Note that the product gLI_L^{th} is the threshold increment of the steady-state SRS gain G_{st}, which must be equal to 25 at $t_L \gg \tau$. In the limit $\tau/t_L \to 0$, expression (16) corresponds approximately to the given normalisation ($gLI_L^{th} \to 22$). A slight deviation from the normalised value (22 instead of 25) is due to the fact that the numerically obtained dependence of gLI_L^{th} on τ/t_L slightly deviates from the linear dependence (16) in the region of large durations ($t_L \gg \tau$), but already at $\tau/t_L < 100$ (or $\tau/t_L > 10^{-2}$) this deviation can be neglected.

Basiev et al. [21] experimentally determined the SRS generation threshold in $BaWO_4$ and $SrWO_4$ crystals of various lengths under picosecond pumping. Comparison of the exper-

imental results with those calculated by formula (16) with account for the g and τ values known for these crystals from [30] shows that their values are close. Thus, for crystals of length greater than 1 cm the discrepancy between theoretical and experimental values does not exceed 8%. For example, for a long $SrWO_4$ crystal ($L = 4.7$ cm), it is only 2%, but for a short $BaWO_4$ crystal ($L = 0.8$ cm) the experimental threshold intensity of SRS generation of the first Stokes component is overestimated by 16% compared with the theoretical value from (16).

It follows from the analysis carried out in [4] that, due partially degenerate four-wave coupling with the first anti-Stokes component, the threshold intensity I_L^{th1} of SRS generation of the first Stokes component exceeds I_L^{th}, defined by a simple two-photon SRS conversion process [formula (16)], if the parameter of the wave detuning of Stokes–anti-Stokes coupling $\Delta k_0 L < 50$, which is fulfilled with decreasing length of the SRS crystal.

We will use a 1.064-μm Nd^{3+}:YAG laser as a pump source and widely known $KGd(WO_4)_2$ ($\nu_R = 901$ cm^{-1}, $g = 4$ cm GW^{-1}, $\tau = 2$ ps) and $Ba(NO_3)_2$ ($\nu_R = 1047$ cm^{-1}; $g = 11$ cm GW^{-1}, $\tau = 27$ ps) crystals [31] as SRS media. Sellmeyer formulas for these crystals are given in [32, 33]. Table 1 shows the wave detunings of FWM processes [calculated by the Sellmeyer formulas using expressions (9) and (10)] for the given crystals at the pump wavelength $\lambda_0 = 1.064$ μm. It was assumed that if in a biaxial $KGd(WO_4)_2$ crystal the light that is polarised parallel to the axis m propagates along the axis p, then the Raman frequency shift is $\nu_R = 901$ cm^{-1} and the refractive index is equal to the principal value n_m of the refractive index tensor.

Figure 2 shows the dependence of the threshold generation intensity of the first Stokes component I_L^{th1} normalised to the threshold of SRS formation I_L^{th} on the SRS crystal length L, obtained by mathematical modelling with equations (6) and (7) for the two given crystals at $\lambda_0 = 1.064$ μm and various pump pulse durations t_L.

One can see from Fig. 2 that I_L^{th1} increases with decreasing L. This dependence on the length of the crystal is due to an increase in the influence of Stokes–anti-Stokes four-wave coupling with decreasing wave detuning parameter $\Delta k_0 L$ [4].

Figure 2 also shows that when the laser pump pulse duration t_L is reduced, the threshold pump intensity I_L^{th1} with decreasing L grows slower, i.e. an increase in the SRS processes nonstationarity reduces the influence of Stokes–anti-Stokes coupling on the SRS threshold.

Table 1. Wave detunings of four-wave coupling of SRS radiation components in $KGd(WO_4)_2$ and $Ba(NO_3)_2$ crystals at the pump wavelength of 1.064 μm.

Wave detuning/cm^{-1}	$KGd(WO_4)_2$	$Ba(NO_3)_2$
Δk_{-2}	63	34
Δk_{-1}	56	29
Δk_0	50	25
Δk_1	42	19
Δk_2	35	13
Δk_3	28	6
Δk_4	18	−6
ΔK_{-2}	119	63
ΔK_{-1}	105	54
ΔK_0	92	44
ΔK_1	78	33
ΔK_2	63	19
ΔK_3	46	−0.5

4. Threshold of Raman-parametric generation of an optical frequency comb

Consider now generation of many SRS components. We are interested in generation of an octave-spanning optical frequency comb when the longest wavelength is approximately 2 times greater than the shortest one. In this case we consider collinear generation of SRS components, which is described by equations (6) and (7), because this process through spatial overlapping of the generated waves can be used for the synthesis of ultrashort pulses – in contrast to the processes of vector Raman-parametric generation, when spaced-apart anti-Stokes cones [14] are generated.

The wavelengths of SRS components are $\lambda_j = (\lambda_0^{-1} - j\nu_R)^{-1}$. For the majority of crystals, the Raman frequency is $\nu_R = 900–1000$ cm^{-1}, while the octave of frequencies corresponds to generation of seven neighbouring SRS components.

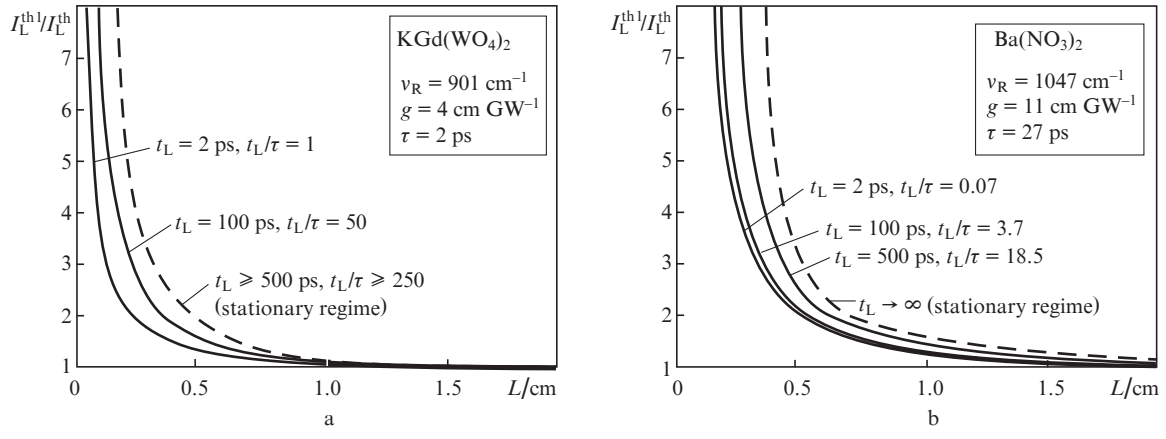

Figure 2. Dependences of the threshold generation intensity of the first Stokes component I_L^{th1} normalised to the threshold of SRS formation I_L^{th} on the SRS crystal length L for the two selected crystals at $\lambda_0 = 1.064$ μm and different values of t_L.

We choose to consider the frequency comb from the second anti-Stokes ($j = -2$) to the fourth Stokes ($j = 4$) components, i.e., in practice, in the case of multi-wave SRS, greater penetration in the Stokes region of the spectrum is commonly observed [5–13].

We assume the generation threshold of the weakest of two extreme SRS components ($j = -2$ or $j = 4$) to be the generation threshold of a frequency comb.

As a result of mathematical modelling by formulas (6) and (7), we obtain the dependences of the threshold generation intensities of the second anti-Stokes [$I_L^{th(-2)}$] and fourth Stokes (I_L^{th4}) SRS components, normalised to the threshold of SRS formation (I_L^{th}) on the SRS crystal length L for the two selected crystals at various laser pump pulse durations t_L. The dependences are shown in Fig. 3.

One can see from Fig. 3 that there is a minimum generation threshold of the second anti-Stokes component, observed at L_{as} = 0.3 and 0.6 cm for $KGd(WO_4)_2$ and $Ba(NO_3)_2$ crystals, respectively. At the same time, the wave detuning $\Delta k_0 L_{as}$ for both crystals is equal to 15, which is optimal for anti-Stokes generation. It is of interest for us that the generation thresholds of the second anti-Stokes and fourth Stokes components, which represent extreme frequencies in the frequency comb, turn out close just near the minimum generation threshold of the second anti-Stokes component; therefore, the minimum generation threshold for the second Stokes wave and the corresponding length of the crystal characterise the conditions that are optimal for achieving the threshold of the entire optical frequency comb generation.

For the $KGd(WO_4)_2$ crystal (Fig. 3a), the minima of the dependences $I_L^{th(-2)}/I_L^{th}$ are 'lifted' by about 1.5 times with increasing laser pump pulse duration from 10 to 100 ps, and for the $Ba(NO_3)_2$ crystal (Fig. 3b), they remain at the same level. This is due to an order larger dephasing time for the $Ba(NO_3)_2$ crystal (27 ps), comparable to the durations of both pump pulses (10 and 100 ps), which is why the SRS process in these cases is transient. At the same time, for the $KGd(WO_4)_2$ crystal with a short dephasing time (2 ps) at a long pump pulse duration (100 ps), the SRS process becomes close to steady-state.

In absolute terms [I_L^{th} is found by formula (16)], the minimum threshold intensities of $I_L^{th(-2)}$ generation at pump pulse durations of 10 and 100 ps are equal to 158 and 100 GW cm^{-2} for the $KGd(WO_4)_2$ crystal and to 264 and 35.4 GW cm^{-2} for the $Ba(NO_3)_2$ crystal. It should be noted that for most SRS crystals under picosecond pumping only the last value is obviously lower than the damage threshold. For example, in experimental papers [20, 21, 34] the damage thresholds for lead molybdate and barium-strontium niobate crystals under 18-ps pumping at 1.064 μm were 40 and 100 GW cm^{-2}, respectively, and for relatively stable crystals of barium and strontium tungstate they were slightly higher. Therefore it is very important to find the optimum conditions for low-threshold multi-wave SRS generation.

We see that in the $Ba(NO_3)_2$ crystal for which the SRS process is transient at both pump pulse durations, the increase in the pulse duration up to 100 ps leads to a sharp decrease (by 7.5 times) in the absolute generation threshold. We can assume that there is an optimal laser pulse duration for the anti-Stokes generation, which lies in the range corresponding to transient SRS, and for the $Ba(NO_3)_2$ crystal it is close to 100 ps. Transition to the steady-state SRS regime does not provide a significant reduction in the absolute threshold of anti-Stokes generation [for the $KGd(WO_4)_2$ crystal it decreases only about 1.5 times].

5. Optimal conditions for Raman-parametric generation of an optical frequency comb

Now we need to determine the conditions of highly efficient SRS generation of an optical frequency comb when all its frequency components overcome the experimental generation threshold, i.e., have a conversion efficiency of $\eta_j > 1\%$.

Figure 4 shows the results of a numerical calculation of the system of equations (6) and (7) for the $Ba(NO_3)_2$ crystal at the pump intensity exceeding the SRS generation threshold by 4 times [i.e., $I_L = 4I_L^{th}$, where I_L^{th} is given by formula (16)], at the pump wavelength λ_0 = 1.064 μm, pump pulse duration t_L = 100 ps and crystal length L = 0.4 cm (Fig. 4a), 0.55 cm (Fig. 4b) and 0.7 cm (Fig. 4c).

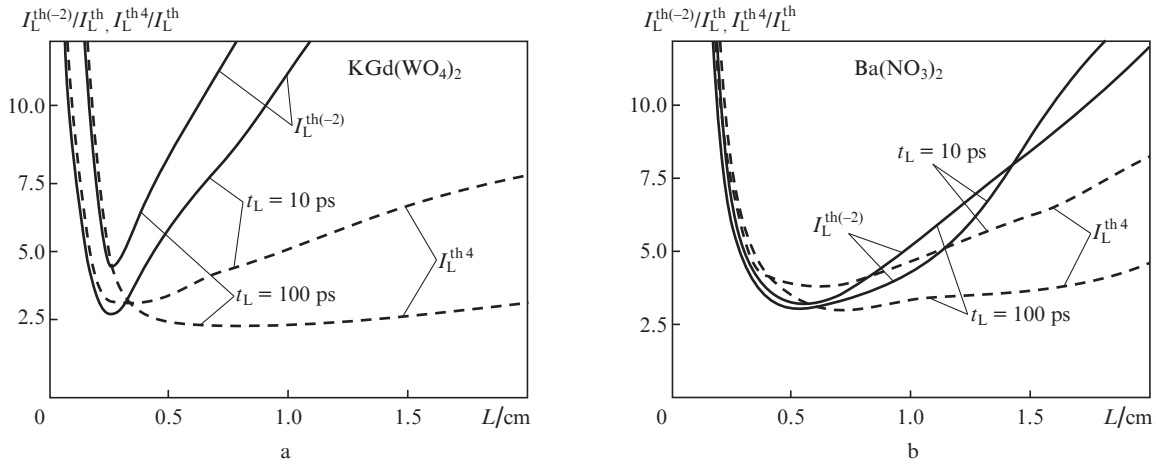

Figure 3. Dependences of the threshold intensities of generation of the second anti-Stokes [$I_L^{th(-2)}$] and fourth Stokes (I_L^{th4}) SRS components normalised to the threshold of SRS formation I_L^{th} on the SRS crystal length L for the two selected crystals at different values of t_L.

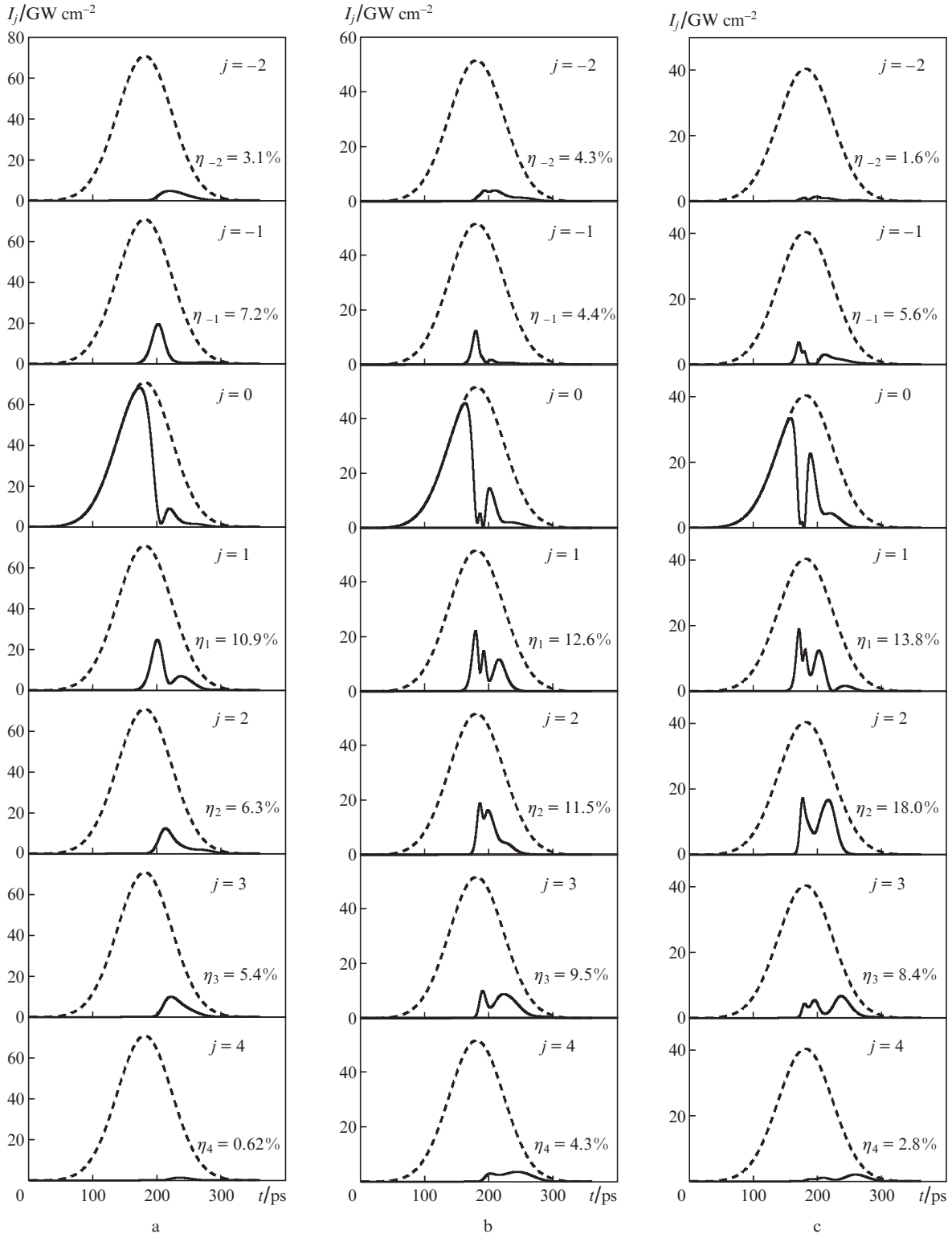

Figure 4. Results of numerical calculation of the system of equations (6) and (7) for the $Ba(NO_3)_2$ crystal at the pump intensity exceeding the threshold of SRS formation by 4 times ($I_L = 4I_L^{th}$), $\lambda_0 = 1.064$ μm, $t_L = 100$ ps and $L =$ (a) 0.4, (b) 0.55 and (c) 0.7 cm.

One can see from Fig. 4 that at a small crystal length ($L = 0.4$ cm), the conversion efficiency into the second anti-Stokes component (the lowest frequency of the frequency comb in question) exceeds the conversion efficiency into the fourth Stokes component (the highest frequency of the frequency comb), but the values of the conversion efficiency are low.

Increasing the length of the crystal up to 0.55 cm (Fig. 4b) provides an increase ($\eta_{-2,4} > 4\%$) and levelling of the conversion efficiencies into the second anti-Stokes and fourth Stokes SRS components. Note that in this case the wave detuning $\Delta k_0 L$ increases to 15, which is close to the optimal value for the Stokes – anti-Stokes coupling.

A further increase in the crystal length to 0.7 cm (Fig. 4c) leads to the fact that the conversion efficiency into the fourth Stokes component is substantially higher than that into the second anti-Stokes component. In this case, the conversion efficiencies into these SRS components decrease as compared to those at $L = 0.55$ cm (Fig. 4b), which is caused by an increase in the wave detuning ($\Delta k_0 L = 18$), leading to a weakening of anti-Stokes FWM generation. Intermediate SRS components ($-2 < j < 4$) in this case contain more energy, but the conversion efficiency into the extreme components of the frequency comb ($j = -2$, and $j = 4$) is low. Consequently, the previous case (Fig. 4b), in which we observed an increase and levelling of the conversion efficiency into extreme components ($j = -2$ and $j = 4$), can be considered optimal for effective Raman-parametric generation of a comb of optical frequencies, i.e., the crystal length $L = 0.55$ cm is optimal for a given pump level $I_L/I_L^{th} = 4$.

Figure 5 shows the calculated dependences of the optimal crystal length L_{opt}, corresponding to equal conversion efficiencies into extreme SRS components of the frequency comb ($\eta_{-2} = \eta_4$), and the most efficient conversion $\eta_{opt} = \eta_{-2} = \eta_4$, corresponding to L_{opt}, on the pump level I_L/I_L^{th} for $Ba(NO_3)_2$ and $KGd(WO_4)_2$ crystals at the pump wavelength $\lambda_0 = 1.064$ μm and pump pulse durations $t_L = 20$ ps (Fig. 5a) and 100 ps (Fig. 5b).

One can see from Fig. 5a that at a low pump pulse duration ($t_L = 20$ ps) in the $KGd(WO_4)_2$ crystal an increase in the pump level I_L/I_L^{th} leads to a rapid increase in the conversion efficiency η_{opt} into the extreme frequency components of the frequency comb (to $\eta_{opt} \approx 8\%$ at $I_L/I_L^{th} = 5$), but the optimal length of the crystal varies slightly and does not exceed 0.5 cm. This is consistent with the experimental results of papers [20, 21], where under 18-ps pumping at 1.064 μm an increase in pump energy in molybdate and tungstate crystals measuring no more than 1 cm in length led to a rapid increase in the conversion efficiencies into high-order SRS components up to fourth one.

In the $Ba(NO_3)_2$ crystal, the generation efficiency η_{opt} (solid curve) at the same low pump pulse duration $t_L = 20$ ps (Fig. 5a) increases very slightly with increasing pump level and at $I_L/I_L^{th} = 5$ does not exceed 0.5%, which is close to the threshold value. In this case, the optimal length of the $Ba(NO_3)_2$ crystal is relatively large ($L_{opt} > 1$ cm).

Note that at $t_L = 20$ ps for the $Ba(NO_3)_2$ crystal we have $t_L/\tau = 0.74$, i.e., a highly transient SRS regime ($t_L < \tau$), and for the $KGd(WO_4)_2$ crystal we have $t_L/\tau = 10$, i.e., an intermediate, transient SRS regime ($\tau < t_L < 100\tau$).

One can see from Fig. 5b that with increasing pump level I_L/I_L^{th} in the $Ba(NO_3)_2$ crystal, the generation efficiency η_{opt} increases rapidly up to 6.5%, while in the $KGd(WO_4)_2$ crystal it increases slowly (dashed line) to a value slightly higher than 1% at $I_L/I_L^{th} = 5$. Note again that at $t_L = 100$ ps for the $Ba(NO_3)_2$ crystal we have $t_L/\tau = 44$, i.e., an intermediate, transient SRS regime, and for the $KGd(WO_4)_2$ crystal we have $t_L/\tau = 50$, i.e., a close-to-steady-state SRS regime.

Note that essentially transient and close-to-steady-state SRS regimes turned to be not optimal for highly efficient Raman-parametric generation of an optical frequency comb.

Figure 6 shows the calculated dependences of the optimal conversion efficiency $\eta_{opt} = \eta_{-2} = \eta_4$ in extreme SRS frequency comb components and the corresponding optimal crystal lengths L_{opt} on the ratio t_L/τ of the laser pump pulse duration to the dephasing time at the pump wavelength $\lambda_0 = 1.064$ μm and pump level $I_L/I_L^{th} = 4$ for $Ba(NO_3)_2$ (solid curves) and $KGd(WO_4)_22$ (dashed curves) crystals.

One can see from Fig. 6 that the behaviour of the dependences for both crystals is similar. A maximum conversion efficiency $\eta_{opt} = \eta_{-2} = \eta_4$ is clearly observed at the ratio $t_L/\tau \approx 10$. In the region of this maximum at $t_L/\tau \approx 10$ we have a shallow minimum of the optimal crystal length, and with a further increase in t_L/τ the optimal crystal length L_{opt} increases slightly (less than by 1.5 times) to a constant value in the region of steady-state SRS ($t_L/\tau > 10^22$).

Additional calculations showed that at other pump levels the position of the conversion efficiency maximum on the t_L/τ axis is still retained, i.e. at any pump level, the octave-spanning SRS generation occurs most effectively when the pump pulse duration is 5-to-20 times higher than the dephasing time of the vibrations of the crystal used.

It should be noted that the region of steady-state SRS ($t_L/\tau > 10^2$) is characterised by a low conversion efficiency η_{opt}

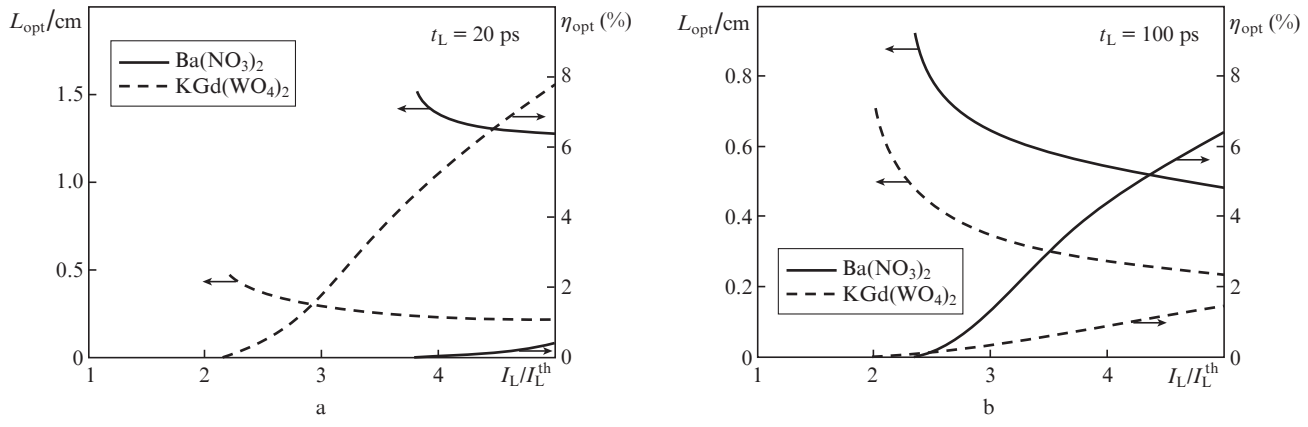

Figure 5. Calculated dependences of the optical crystal length L_{opt} corresponding to equal conversion efficiencies into extreme SRS components of the frequency comb, as well as of the conversion efficiency $\eta_{opt} = \eta_{-2} = \eta_4$ corresponding to L_{opt} on the pump level I_L/I_L^{th} for the $Ba(NO_3)_2$ and $KGd(WO_4)_2$ crystals at $\lambda_0 = 1.064$ μm and $t_L =$ (a) 20 and (b) 100 ps.

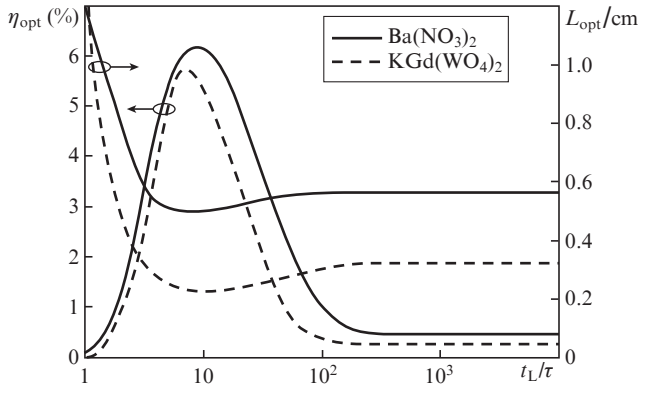

Figure 6. Calculated dependences of the optimal conversion efficiency $\eta_{opt} = \eta_{-2} = \eta_4$ into extreme frequency comb SRS components and optimal crystal length L_{opt} on the ratio of the laser pump pulse duration to the dephasing time t_L/τ at $\lambda_0 = 1.064$ μm and pump level $I_L/I_L^{th} = 4$ for $Ba(NO_3)_2$ and $KGd(WO_4)_2$ crystals.

(tenths of a percent), in contrast to the region of highly transient SRS ($t_L/\tau < 1$), where η_{opt} drops almost to zero (more precisely, to ~0.01%). This explains the failure of Losev et al. [35] to implement multi-wave SRS in the $KGd(WO_4)_2$ crystal at a nonoptimal pump pulse duration $t_L = 0.15$ ps. Only an increase (with chirping) in pump pulse duration to 2 ps and more made it possible to realise Raman-parametric generation of multiple SRS components in the present paper.

6. Conclusions

Thus, we have studied theoretically the conditions of low-threshold collinear optical frequency comb generation under transient (picosecond) SRS and parametric four-wave coupling of SRS components in crystals.

Raman-parametric generation of an octave-spanning optical frequency comb is shown to occur most effectively in the intermadiate, transient SRS regime when the pump pulse duration is 5-to-20 times greater than the dephasing time of vibrations of the crystal used.

For the intermediate, transient regime, which corresponds to the pump pulse duration exceeding the dephasing time, we have found a simple approximation dependence of the threshold intensity of SRS formation on the parameters of the SRS medium and pump radiation. Using the dependence obtained we have analysed the thresholds Raman-parametric generation of many SRS components making up the frequency comb.

We have found the optimal values of not only the laser pump pulse duration, but also the SRS crystal length corresponding to highly efficient generation of an optical frequency comb from the second anti-Stokes component to the fourth Stokes SRS component inclusive. For the $KGd(WO_4)_2$ (high-dispersion) and $Ba(NO_3)_2$ (low-dispersion) crystals in question, the optimal crystal length L was 0.3 and 0.6 cm at a pump wavelength of 1.064 μm and pulse duration greater than the dephasing time by 5 times or more, which corresponds to the condition of the most effective anti-Stokes-Stokes coupling $\Delta kL \approx 15$, where Δk is the wave detuning of phase matching of Stokes–anti-Stokes coupling, determined by the dispersion of the refractive index of the SRS medium.

Acknowledgements. The author thanks A.A. Kaminskii for discussion of the results. This work was partially supported by the Russian Foundation for Basic Research (Grant No. 13-02-00031).

References

1. Shen Y.R. *The Principles of Nonlinear Optics* (New York: John Wiley & Sons, 1984; Moscow: Nauka, 1989).
2. Gorelik V.S., Sushchinskii M.M. *Usp. Fiz. Nauk*, **98**, 237 (1969).
3. Lisinetskii V.A., Rozhok S.V., Bus'ko D.N., Chulkov R.V., Grabtchikov A.S., Orlovich V.A., Basiev T.T., Zverev P.G. *Laser Phys. Lett*., **2**, 396 (2005).
4. Basiev T.T., Smetanin S.N., Shurygin A.S., Fedin A.V. *Usp. Fiz. Nauk*, **180**, 639 (2010) [*Phys. Usp*., **53**, 611 (2010)].
5. Losev L.L., Lutsenko A.P. *Kvantovaya Elektro*n., **20**, 1054 (1993) [*Quantum Electron*., **23**, 919 (1993)].
6. Eimerl D., Milam D., Yu J. *Phys. Rev. Lett*., **70**, 2738 (1993).
7. Kawano H., Hirakawa Y., Imasaka T. *Appl. Phys. B*, **65**, 1 (1997).
8. Turner F.C., Trottier A., Strickland D., Losev L.L. *Opt. Commun*., **270**, 419 (2007).
9. Kaminskii A.A., Bagayev S.N., Grebe D., Eichler H.J., Pavlyuk A.A., Macdonald R. *Kvantovaya Elektron*., **23**, 199 (1996) [*Quantum Electron*., **26**, 193 (1996)].
10. Kaminskii A.A., Becker P., Bohaty L., Ueda K., Takaichi K., Hanuza J., Maczka M., Eichler H.J., Gad G.M.A. *Opt. Commun*., **206**, 179 (2002).
11. Kaminskii A.A., Bohaty L., Becker P., Held P., Rhee H., Eichler H.J., Hanuza J. *Laser Phys. Lett*., **6**, 335 (2009).
12. Kaminskii A.A., Lux O., Rhee H., Eichler H.J., Ueda K., Yoneda H., Shirakawa A., Zhao B., Chen J., Dong J., Zhang J. *Laser Phys. Lett*., **9**, 879 (2012).
13. Kaminskii A.A., Lux O., Rhee H., Eichler H.J., Yoneda H., Shirakawa A., Ueda K., Ruckamp R., Bohaty L., Becker P. *Laser Phys. Lett*., **10**, 1 (2013).
14. Bloembergen N. *Am. J. Phys*., **35**, 989 (1967).
15. Chiao R.Y., Stoicheff B.P. *Phys. Rev. Lett*., **12**, 290 (1964).
16. Hickman A.P., Bischel W.K. *Phys. Rev. A*, **37**, 2516 (1988).
17. McDonald G.S., New G.H.C., Losev L.L., Lutsenko A.P., Shaw M. *Opt. Lett*., **19**, 1400 (1994).
18. Butylkin V.S., Venkin G.V., Protasov V.P., Smirnov N.D., Khronopulo Yu.G., Shalyaev M.F. *Pis'ma Zh. Eksp. Teor. Fiz*., **17**, 400 (1973) [*JETP Lett*., **17**, 285 (1973)].
19. Butylkin V.S., Venkin G.V., Protasov V.P., Fisher P.S., Khronopulo Yu.G., Shalyaev M.F. *Zh. Eksp. Teor. Fiz*., **70**, 829 (1976) [*Sov. Phys. JETP*, **43**, 430 (1976)].
20. Basiev T.T., Doroshenko M.E., Smetanin S.N., Jelinek M. Jr., Kubecek V., Jelinkova H., Shekhovtsov A.N., Kosmyna M.B. *Laser Phys. Lett*., **9**, 853 (2012).
21. Basiev T.T., Doroshenko M.E., Ivleva L.I., Smetanin S.N., Jelínek M., Kubeček V., Jelínková H. *Kvantovaya Elektron*., **43**, 616 (2013) [*Quantum Electron*., **43**, 616 (2013)].
22. Auston D., in *Ultrashort Light Pulses*. Ed. by S.L. Shapiro (Berlin: Springer, 1977; Moscow: Mir, 1981).
23. Akhmanov S.A., Drabovich K.N., Sukhorukov A.P., Chirkin A.S. *Zh. Eksp. Teor. Fiz*., **59**, 485 (1970) [*Sov. Phys. JETP*, **32**, 266 (1971)].
24. Raymer M.G., Mostowski J. *Phys. Rev. A*, **24**, 1980 (1981).
25. Von der Linde D., Maier M., Kaiser W. *Phys. Rev*., **178**, 11 (1969).
26. Dzhidzhoev M.S., Mikheev P.M., Platonenko V.T., Savel'ev A.V. *Kvantovaya Elektron*., **24**, 255 (1997) [*Quantum Electron*., **27**, 249 (1997)].
27. Basiev T.T., Osiko V.V., Prokhorov A.M., Dianov E.M. *Topics Appl. Phys*., **89**, 351 (2003).
28. Smetanin S.N., Doroshenko M.E., Ivleva L.I., Jelínek M., Kubeček V., Jelínková H. *Appl. Phys. B*, **117**, 225 (2014).
29. Carman R.L., Shimizu F., Wang C.S., Bloembergen N. *Phys. Rev. A*, **2**, 60 (1970).
30. Basiev T.T. *Fiz. Tverd. Tela*, **47**, 1354 (2005) [*Phys. Sold. State*, **47**, 1400 (2005)].
31. Basiev T.T., Zverev P.G., Karasik A.Ya., Osiko V.V., Sobol' A.A., Chunaev D.S. *Zh. Eksp. Teor. Fiz*., **126**, 1073 (2004) [*JETP*, **99**, 934 (2004)].

32. Pujol M.C., Rico M., Zaldo C., Sole R., Nikolov V., Solans X., Aguilo M., Diaz F. *Appl. Phys. B*, **68**, 187 (1999).
33. Zverev P.G., Basiev T.T., Osiko V.V., Kulkov A.M., Voitsekhovskii V.N., Yakobson V.E. *Opt. Mater*., **11**, 315 (1999).
34. Basiev T.T., Doroshenko M.E., Ivleva L.I., Smetanin S.N., Jelínek M., Kubeček V., Jelínková H. *Laser Phys. Lett*., **10**, 519 (2013).
35. Losev L.L., Song J., Xia J.F., Strickland D., Brukhanov V.V. *Opt. Lett*., **27**, 2100 (2002).